energy&fuels

Article

pubs.acs.org/EF

Impact of Laboratory-Induced Thermal Maturity on Asphaltene Molecular Structure

Andrew E. Pomerantz,*[,†] Tuong Van Le Doan,[†] Paul R. Craddock,[†] Kyle D. Bake,[†] Robert L. Kleinberg,[†] Alan K. Burnham,[‡] Qinghao Wu,[§] Richard N. Zare,[§] Grant Brodnik,[∥] William Chung Hei Lo,[∥] Michael Grayson,[∥] Sudipa Mitra-Kirtley,[∥] Trudy B. Bolin,[⊥,#] and Tianpin Wu[⊥]

[†]Schlumberger-Doll Research, Cambridge Massachusetts 02139, United States

[‡]Department of Energy Resources Engineering, Stanford University, Stanford California 94305, United States

[§]Department of Chemistry, Stanford University, Stanford California, 94305, United States

[∥]Rose-Hulman Institute of Technology, Terre Haute Indiana 47803, United States

[⊥]Argonne National Laboratory, Argonne Illinois 60439, United States

ABSTRACT: The structure of asphaltenes of various maturities prepared by semiopen pyrolysis of Green River Shale is measured by elemental analysis, laser desorption laser ionization mass spectrometry (L^2MS), surface assisted laser desorption ionization (SALDI) mass spectrometry, sulfur X-ray absorption near edge structure (XANES) spectroscopy, and infrared (IR) spectroscopy. These measurements demonstrate systematic changes in the composition of asphaltenes during thermal maturation. At low maturities, the evolution of asphaltene composition is dominated by changes in the heteroatoms: total sulfur as well as carbon−oxygen, sulfur−oxygen (sulfoxide), and aliphatic carbon−sulfur (sulfide) bonds are lost, while the molecular weight increases. At high maturities, the sulfur content and speciation as well as molecular weight are relatively constant while the evolution in composition is dominated by changes in the carbon backbone: the abundance of aromatic relative to aliphatic carbon increases, the length of aliphatic chains shortens, and the abundance of aromatic C−H bonds increases greatly. The distribution of different carbon−oxygen functional groups is relatively unchanged over the entire maturity range. These changes sometimes mirror and sometimes oppose compositional changes in the bitumen, suggesting that the composition of the asphaltene and maltene fractions of bitumen evolve differently. The observed changes in asphaltene structure are not fully independent of one another, as the composition of asphaltenes is constrained to maintain a balance of the strength of intermolecular forces to ensure solubility in aromatic solvent and insolubility in aliphatic solvent (the definition of asphaltenes). That constraint leads to a decrease in sulfoxide content (weakening intermolecular forces by reducing dipole interactions) concurrent with an increase in molecular weight (strengthening intermolecular forces). These trends in asphaltene composition with maturity are expected to occur in naturally occurring source rocks, such as some tight-oil formations, but not necessarily in conventional reservoir rocks where the asphaltenes escape from the source rock and enter the reservoir during maturation.

INTRODUCTION

The chemical composition of organic matter in source and reservoir rocks can vary greatly, reflecting the processes involved during different phases of sedimentation, diagenesis, and petroleum generation. Organic matter is typically classified into several categories, although the definitions vary somewhat. In this paper, kerogen and bitumen are defined as the portions of organic matter that are insoluble and soluble, respectively, in organic solvents, while oil and gas are expellable from the source rock and the former is liquid at standard conditions.[1] The distinction between oil and bitumen using these definitions depends on the transport mechanisms available for expulsion from the source rock, and the fractionation can differ between laboratory experiments and nature.[2] The relative abundance of those different components varies with processes such as maturity (the extent of thermal transformation): organic matter in immature source rocks is mostly kerogen, medium maturity source rocks contain abundant bitumen, and higher maturity source rocks are rich in oil and gas.[1,3] The composition of the individual classes varies as well. For example, in kerogen the atomic H/C ratio can range 0.5−1.5, the aromaticity can range 20−90%, and the atomic O/C ratio can range 0.05−0.15 depending on organic matter input and depositional environment (which impacts the kerogen type) and maturity.[4,5] Bitumen can exhibit similar trends in aromaticity[6] and hydrogenated and oxygenated functional groups,[7] as well as variation in sulfur speciation from mainly oxidized forms to mainly reduced forms.[3,8] Produced fluids vary from dry gas to liquids rich in asphaltenes based on the source and maturity as well as postgenerational processes such as biodegradation.[9,10] These processes typically impact specific molecules (including biomarkers) in addition to bulk composition.[10]

The impact of these processes on asphaltenes, the fraction that is soluble in aromatic solvents such as benzene or toluene but insoluble in aliphatic solvents such as pentane or heptane, in the past has been difficult to assess because of difficulties in measuring the composition of asphaltenes.[11,12] Much of the difficultly in studying asphaltenes can be attributed to their

Received: May 23, 2016
Revised: July 21, 2016
Published: July 26, 2016

DOI: 10.1021/acs.energyfuels.6b01238
Energy Fuels 2016, 30, 7025−7036

tendency to aggregate, leading to challenges in data interpretation. Several techniques have now been demonstrated to provide accurate and unbiased measurement of the molecular and colloidal structure of asphaltenes,[13] culminating in the Yen-Mullins model of asphaltene molecules and aggregates.[14,15] This model is now used to interpret various observations such as spatial gradients in the asphaltene concentration of crude oil in a reservoir[16−24] and asphaltene interfacial activity.[25]

As described by the Yen-Mullins model, asphaltenes from conventional petroleum reservoirs are composed predominantly of single aromatic cores with alkyl side chains in molecules with an average weight near 700 Da. This structure is supported by numerous experiments including time-resolved fluorescence depolarization (TRFD),[26,27] laser desorption laser ionization mass spectrometry (L^2MS),[28−33] laser desorption/ionization (LDI) mass spectrometry,[34−36] multistage tandem mass spectrometry,[37] optical spectroscopy with molecular orbital calculations,[38,39] NMR spectroscopy,[40−42] and atomic force microscopy.[43] Compared to the wide variations in composition found in kerogen and bitumen from source rock, these measurements indicate little variation in the composition of asphaltenes from reservoir rock. Relative consistency of conventional petroleum asphaltenes had been noted in earlier studies, which found that the atomic H/C ratio of asphaltenes from many reservoir rocks generally lies in the narrow range centered around 1.15.[44]

Recently, a series of semiopen pyrolysis experiments were performed on Green River Shale, in which immature oil shale was pyrolyzed to different extents, producing a suite of samples at various maturities. Systematic effects of the maturity variation were observed in the composition of the organic matter, particularly the kerogen and bitumen phases.[3,6,7] In these experiments, bitumen was the primary product from kerogen breakdown at relatively low maturities and at higher maturities broke down itself to form the majority of the produced fluids. Moreover, the composition of the bitumen phase varied with maturity: the pyrolysis process altered the H/C ratio, aromaticity, alkane chain distribution, oxygenated functional group abundance, sulfur content, and sulfur speciation.[3,6,7] Because the asphaltene content of bitumen is relatively high,[3] these results raise the hypothesis that the composition of the asphaltenes themselves may vary with maturity to a larger extent than typically observed in asphaltenes from reservoir rocks.

To test that hypothesis, here the asphaltenes from the Green River pyrolysis experiments are isolated and analyzed using many of the same techniques applied earlier to asphaltenes from reservoir rocks: elemental analysis, laser desorption laser ionization mass spectrometry (L^2MS) to measure molecular weight, surface assisted laser desorption ionization (SALDI) mass spectrometry to measure nanoaggregate weight, sulfur X-ray absorption near edge structure (XANES) spectroscopy to measure sulfur speciation, and infrared (IR) spectroscopy to measure functional group abundances. The results are interpreted to understand how the composition of these source-rock asphaltenes evolve with maturity.

MATERIALS AND METHODS

Oil Shale Samples. Pyrolysis was performed on Green River oil shale samples from the R-1 zone of the Garden Gulch member. These samples have been described in detail previously.[3,45] Briefly, the samples contain immature Type I kerogen and are rich in organic carbon (13 wt % total organic carbon). The samples were collected as cuttings from a well drilled with a reverse circulation drilling method using naturally occurring groundwater and air to transport the cuttings to the surface, so no drilling fluid contamination was present. Once received, the samples were ground to a particle size of 100−200 μm, homogenized, and split to ensure identical starting material for each pyrolysis experiment.

Pyrolysis Experiments. The Green River samples were pyrolyzed in a semiopen self-purging reactor, designed to simulate *in situ* processing of oil shale.[3] Pyrolysis involved rapid heating from room temperature to 180 °C, slower heating (heating rate = 2−120 °C/h) to a plateau temperature (300−435 °C), followed by an isothermal soak (5−12.5 h). Pressure was held constant (1−5 MPa) by an automatic valve system that released vapors as they were generated. At the conclusion of the experiment, pressure was reduced to ambient.

The severity of pyrolysis for the different experiments is computed based on thermal history using the EASY%Ro algorithm.[46] The EASY%Ro method models vitrinite maturation based on the amount of heat to which the shale has been exposed. The model uses Arrhenius first-order parallel-reaction kinetics with a distribution of activation energies. The extent of maturation is reported in units of the traditional vitrinite reflectance measurement, and the calculated EASY%Ro maturities can be compared to vitrinite reflectance measurements, even for samples where direct vitrinite reflectance measurements are not possible. As a result, the maturity of these samples is expressed in familiar vitrinite reflectance units, although the correspondence between laboratory and natural reflectance maturation should not be considered exact. The maturity of the native state shale is 0.48% EASY%Ro, resulting from natural maturation in the subsurface.[3] The pyrolysis experiments reported here matured the samples to the range 0.78−1.28% EASY%Ro.

Organic matter is partitioned into several phases. Kerogen is defined as the nonvolatile and insoluble organic matter; it remains in the reactor during pyrolysis and cannot be subsequently extracted by organic solvent. Bitumen is defined as the nonvolatile and soluble organic matter; it remains in the reactor during pyrolysis but is subsequently extracted by Soxhlet extraction using 9:1 dichloromethane/methanol. Oil and gas are the components that are expelled from the reactor during pyrolysis and subsequently separated with a condenser. Figure 1 shows the relative abundance of each organic phase from the pyrolysis experiments. At intermediate maturities, bitumen comprises most of the organic matter. These experiments span a sufficient range in maturity to include samples where the organic matter is dominated by kerogen (low maturity), bitumen (moderate maturity), and oil plus gas (high maturity).

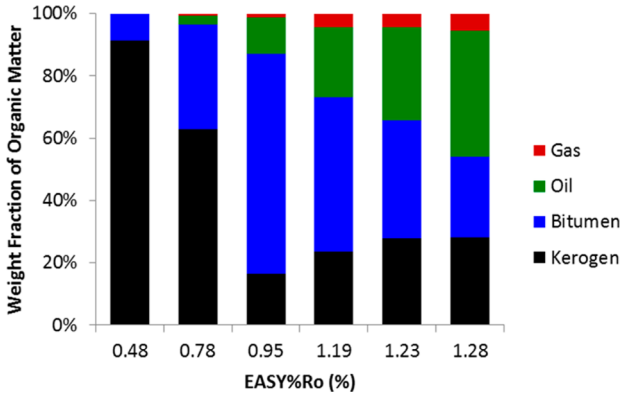

Figure 1. Distribution of organic products from the pyrolysis experiments.

Asphaltene Isolation. Asphaltenes in these pyrolysis experiments partition primarily into the bitumen phase due to their low volatility. To extract asphaltenes, the bitumens were diluted 1:40 in *n*-pentane, and the mixture was stirred overnight to allow the asphaltenes to precipitate. The solution was then vacuum filtered using a Teflon

DOI: 10.1021/acs.energyfuels.6b01238
Energy Fuels 2016, 30, 7025−7036

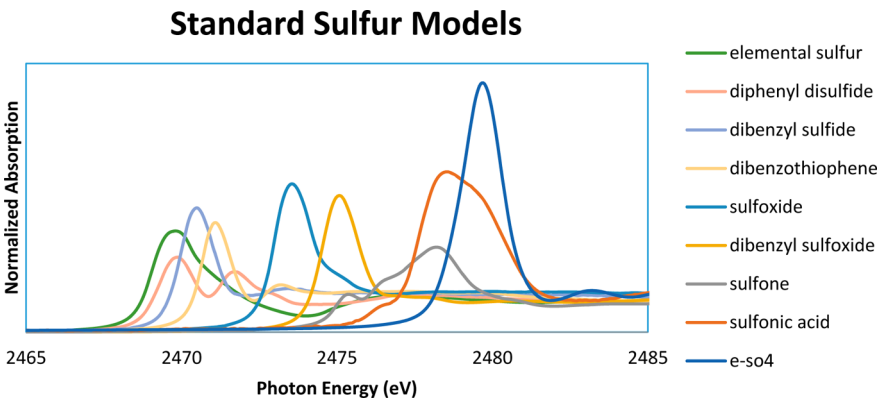

Figure 2. XANES plots of sulfur model compounds. The main peak shifts to higher photon energies as the formal oxidation number of sulfur increases. Potassium sulfate is labeled as "e-so4".

membrane with 0.47 μm pores. The asphaltene precipitate was collected as a dry powder then further purified by extracting residual pentane-soluble material in a Soxhlet extractor. After extraction, the purified asphaltenes were allowed to dry in a fume hood. The isolated asphaltenes were subsequently verified to be soluble in toluene, confirming that they meet the traditional definition of asphaltenes (benzene or toluene soluble, pentane or heptane insoluble).

Elemental Analysis. Carbon, hydrogen, and sulfur concentrations were measured by traditional combustion-based elemental analysis.

Laser Desorption Laser Ionization Mass Spectrometry (L^2MS). L^2MS has been used frequently to measure the molecular weight of asphaltenes.[28−32,47−50] L^2MS involves two spatially and temporally separated lasers to desorb and subsequently ionize asphaltenes, followed by mass analysis of the ions. Desorption is accomplished by an infrared laser that heats the analyte at approximately 10^8 K/s, leading to thermal desorption without fragmentation or ionization.[51] Ionization of the desorbed neutrals is accomplished by single photon vacuum ultraviolet ionization, a nearly universal soft ionization technique that ionizes all analytes of appropriate ionization potential.[52] A small delay between the desorption and ionization laser pulses allows the neutrals to disperse in the vacuum, minimizing the ion-induced dipole attractive forces that cause aggregation in single laser mass spectrometry.[53] Mass analysis is accomplished by a time-of-flight mass analyzer, which offers modest mass accuracy and resolution but provides a nearly constant sensitivity across a wide mass range.[54] A recent analysis of all steps in the measurement process demonstrated that L^2MS provides an accurate and unbiased measurement of asphaltene molecular weight, without particularly high or low sensitivity to polar species, strongly aggregating species, or any other known fraction of asphaltenes.[33]

The methods used for the L^2MS experiments are similar to those described previously.[48,50] Briefly, a small amount of asphaltene is fixed on a copper platter with double-sided tape and transferred into a vacuum chamber through a vacuum interlock. A pulse of IR radiation from a CO_2 laser (λ = 10.6 μm; Alltec GmbH, model AL 882 APS) is focused to a spot (~50 μm in diameter) on the sample surface using a Cassegrainian microscope objective (Ealing Optics, 15×). Desorbed neutral molecules from the platter surface form a plume in the extraction region of a time-of-flight mass spectrometer (TOF-MS). After a brief delay, this plume is intersected perpendicularly by the vacuum ultraviolet (VUV) output of a pulsed F_2 excimer laser (λ = 157 nm; Coherent, Inc., ExciStar XS 200, Selmsdorf, Germany) and is ionized through single photon ionization (SPI). The created ions are analyzed in a home-built linear TOF-MS. Each recorded spectrum is averaged over 100 laser shots.

Surface Assisted Laser Desorption Ionization (SALDI) Mass Spectrometry. Unlike the two-laser process involved in L^2MS, SALDI employs a single laser and an activated surface to accomplish desorption and ionization simultaneously. As a result, ion-induced dipole interactions are not suppressed, and analytes can be detected as aggregates.[48−50] Asphaltenes can exist in multiple forms of aggregates, and SALDI detects asphaltenes in the nanoaggregate form described by the Yen-Mullins model.[14,15] The nanoaggregate consists of approximately 6−8 molecules and is the smallest form of asphaltene aggregate. Because asphaltene nanoaggregates are weakly held together, they are detectable only when low laser pulse energies are used in SALDI measurements; at high energies, the nanoaggregate dissociates and asphaltenes are detected as smaller multimers or individual molecules.[33]

The methods used for the SALDI experiments are similar to those described previously.[49,50] Briefly, SALDI mass spectra were obtained using a PCS4000 mass spectrometer (Bio-Rad, Fremont, CA). Nonselective normal phase NP20 arrays (Ciphergen, Fremont, CA) were used. The surface of the arrays was modified by silicon oxide groups, which may assist with desorption/ionization. A pulsed nitrogen laser with a wavelength of 337 nm was used to desorb and ionize the asphaltenes. The laser pulse energy was scanned from 1000 to 6000 nJ/pulse in steps of 250 nJ for each sample, and spectra were obtained using conditions maximizing the intensity of the nanoaggregate signal. Data were acquired in the positive-ion mode from m/z 0 to 20 000, focused at 4000 Da. To introduce the samples into the mass spectrometer, the asphaltenes were dissolved in toluene to form 2 mg/mL solutions. These solutions were used to obtain surface concentrations of 96 μg/cm^2 by depositing a drop of 2 μL solution onto a spot (outer diameter of 2.3 mm) on the array. The data analysis was performed using ProteinChip and Ciphergen Express software. The baseline was subtracted using the following settings: smooth before fitting baseline with 25 points and fit with 100 times expected peak width. Filtering was "on" using an average width of 0.2 times the expected peak width.

Sulfur K-Edge X-ray Absorption Near Edge Structure (XANES) Spectroscopy. Sulfur K-edge XANES measures the distribution of sulfur-containing functional groups in nonvolatile hydrocarbon mixtures such as coal,[55−57] kerogen,[4,8,58,59] bitumen,[8,60] asphalts,[61] and asphaltenes.[62−66] As applied here, XANES measures transitions from electrons in sulfur 1s orbitals to molecular orbitals with significant 3p character.[67,68] The transition energies depend on the bonding environment of the sulfur nucleus, enabling XANES to resolve different forms of sulfur such as sulfide (sulfur bonded to aliphatic carbon), thiophene (sulfur bonded to aromatic carbon), and sulfoxide (sulfur double bonded to oxygen).[64,69] Resolving sulfur forms of similar oxidation state by XANES can be challenging.[70,71] Sulfur speciation is of interest in many sections of the petroleum industry because it impacts the kinetics of oil generation,[72] the transport of oil in reservoirs,[8] the formation of compositional gradients in crude oil,[63] the process of oil refining,[73] and the stability of asphalt surfaces.[61]

The sulfur K-edge XANES data were collected at the bending magnet beamline 9-BM at Advanced Photon Source (APS), Argonne National Laboratory. The range of photon energies used in the experiments was from 2450 to 2600 eV, using a Si[111] double crystal monochromator. The samples were placed in a helium atmosphere to

DOI: 10.1021/acs.energyfuels.6b01238
Energy Fuels 2016, 30, 7025−7036

mitigate air absorption. A Lytle detector was used for fluorescence data collection.

The standard models used for the experiment were elemental sulfur, dibenzyl sulfide, diphenyl disulfide, dibenzothiophene, dibenzyl sulfoxide, dimethyl sulfoxide, diphenyl sulfoxide, diphenyl sulfone, isethionic acid, sulfonic acid, and potassium sulfate. Sodium thiosulfate was used as the energy calibration sample for all the measurements, with its lowest K-edge feature at 2469.2 eV.[74] The asphaltene samples were diluted in toluene to about 1% sulfur by weight to eliminate any possible self-absorption effects. The liquid samples were mounted in the sample holder in small polycarbonate packets, directly in the path of the beam. All spectra were background-subtracted and then normalized at the same post-XANES photon energy.

Figure 2 shows a plot of all the models that were used in the XANES analysis. As the formal oxidation number of sulfur of the model structures increases, the main peak shifts to higher energies, enabling the identification and quantitative analysis of the different sulfur structures in the asphaltene samples. Each asphaltene spectrum was fitted with a database of spectra of the model compounds, and the relative abundances of the different sulfur structures in each asphaltene sample were determined.

Infrared (IR) Spectroscopy. IR spectroscopy measures the distribution of vibrational frequencies of an analyte, which can be interpreted to estimate the relative abundance of different functional groups. IR spectroscopy has been used to measure the composition of nonvolatile hydrocarbon mixtures such as soils and sediments,[75] coals,[76−78] kerogens,[7,79−82] bitumens,[7] asphalts,[83] and asphaltenes.[80,84,85] Multiple functional groups are routinely identified and quantified, including aliphatic CH, CH_2, and CH_3; aromatic CH and CC; and oxygenated functionalities such as carboxyl, quinone, aldehyde, ketone, and ester.[76,86]

The IR spectra were acquired on splits of the isolated asphaltenes prepared as KBr pellets. This method allows the mass of sample and KBr matrix to be carefully controlled and has been shown to yield IR spectra of organic materials that can be interpreted quantitatively according to the Beer−Lambert Law.[7] The asphaltenes were gently ground by hand in an organic-clean mortar to disaggregate large asphaltene aggregates. Precisely 5.00 ± 0.01 mg of asphaltene was added to a clean, 5 mL tungsten carbide mixing vial containing two 7 mm diameter agate spheres. Precisely 900.0 ± 0.5 mg of KBr was then weighed out. The KBr was supplied as a powder (XL Spectrograde, International Crystal Laboratories, Garfield, NJ) and heated overnight (16 h, 450 °C) prior to use to remove organic impurities. The KBr was added and mixed with the asphaltene in increments to provide effective grinding and homogeneous distribution of the asphaltene in the KBr suspension. For this mixing procedure, a mass of KBr equivalent to the mass of asphaltene was first added to the mixing vial. The components were mixed for 5 min at 23 Hz using a Retsch MM400 mixer mill (Verder Scientific Inc., Newtown, PA). Subsequent additions of KBr were made by adding a mass of KBr approximately equal to the mass of the mixture in the mixing vial. In total, six additions were made for a combined mixing time of 30 min. Next, 200.0 ± 0.5 mg of the homogeneous, powdered mixture was split and pressed into a clear, 13 mm diameter pellet using a prepared die under vacuum at 10 tons/cm^2 for 10 min. The prepared pellet was stored in a vacuum oven at 100 °C until FTIR analysis.

The asphaltene FTIR spectra were acquired in transmission mode using a Bruker Vertex70 dual-range spectrometer. The measurement comprised 25 individual scans across the mid-IR range (5200−450 cm^{-1}) lasting 2 s each. The spectral resolution for each scan was 2 cm^{-1}. The FTIR spectrum was computed as the average absorption spectrum of the 25 scans. A background mid-IR spectrum was collected at the beginning of each measurement and automatically removed from the asphaltene IR spectrum prior to interpretation of the spectra.

RESULTS

Photography. Figure 3 presents photographs of the isolated asphaltene samples. Their color exhibits a clear trend

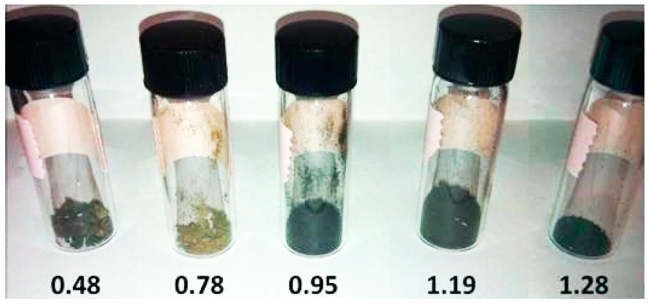

Figure 3. Photograph of the asphaltenes samples, labeled by their maturity.

from brown at lower maturities to black at high maturities. Color in carbonaceous materials reflects the aromatic structure, with a deeper black color indicating greater aromaticity and larger fused ring systems.[38,87,88] These trends identified qualitatively by visual inspection are consistent with the quantitative trends determined by various spectroscopic measurements as discussed below.

Elemental Analysis. Figure 4 presents the elemental analysis of the asphaltene samples. Clear trends with maturity

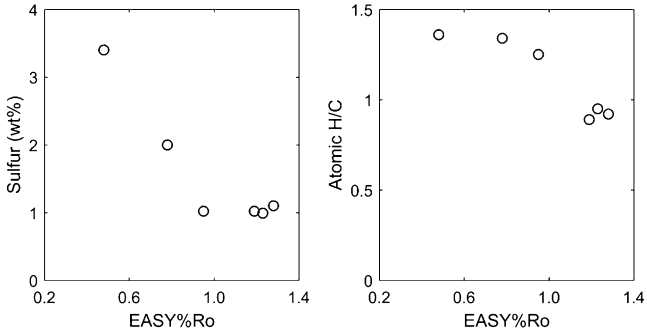

Figure 4. Elemental analysis of the asphaltene samples.

are observed in both the sulfur content and the H/C ratio. Sulfur content decreases from 3.4 wt % to 1.0 wt % with maturity early in the maturation process and then stabilizes around 1.0 wt % at higher maturities. Conventional petroleum asphaltenes from different locations span a wide range of sulfur contents, and the sulfur contents of these samples all lie within that range.[44] The H/C ratio of these pyrolysis asphaltenes decreases smoothly over the entire maturity range studied, falling from 1.36 at the lowest maturity to 0.92 at the highest. By comparison, the average H/C for petroleum asphaltenes from conventional reservoirs has been estimated at 1.14.[9] A collection of petroleum asphaltenes from a large number of conventional deposits has an average H/C of 1.13 and a standard deviation of 0.11.[44] Asphaltenes from some areas can be more compositionally diverse. For example, petroleum asphaltenes from the Northern Viking Graben area in the Norwegian North Sea were found to range from 0.9 to 1.5 in H/C ratio.[89] The asphaltenes studied here are sourced from Type I kerogen, while conventional petroleum deposits are usually sourced by Type II kerogen, suggesting that the asphaltenes studied here would not necessarily be expected to be compositionally similar to typical asphaltenes from conventional petroleum reservoirs. Previous analysis of naturally occurring asphaltenes from areas similar to that studied here have relatively high H/C ratios: 1.30 for asphaltenes from the

DOI: 10.1021/acs.energyfuels.6b01238
Energy Fuels 2016, 30, 7025−7036

Sunnyside tar sand,[90] 1.36 for asphaltenes from Gilsonite deposits in the Bonanza area in eastern Utah,[91] and 1.67 for asphaltenes from immature Green River Shale from an unspecified location.[92] The H/C ratios of the unpyrolyzed (EASY%Ro = 0.48%) and low maturity (EASY%Ro = 0.78%) samples studied here is consistent with that literature.

Laser Desorption Laser Ionization Mass Spectrometry (L^2MS). The L^2MS spectra of the asphaltene samples are presented in Figure 5. Asphaltenes are a complex mixture

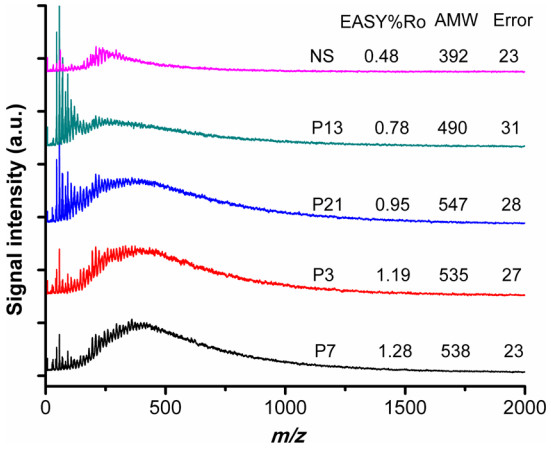

Figure 5. L^2MS spectra of the asphaltene samples. Samples are labeled by their EASY%Ro, and the average molecular weight (AMW) and its standard deviation (both in g/mol) are listed.

whose individual components are not resolved by L^2MS, so the mass spectra appear as broad distributions lacking discrete peaks. Some individual peaks are detected at low mass, which correspond to fragments. Those peaks are narrow (in part because the resolution of the time-of-flight mass spectrometer is relatively high at low mass) and do not significantly impact the quantitative interpretation of the data.[33] The data are quantitatively interpreted by computing the number-average molecular weight (Figure 6). The number-average molecular weight increases from approximately 400 g/mol at low maturity

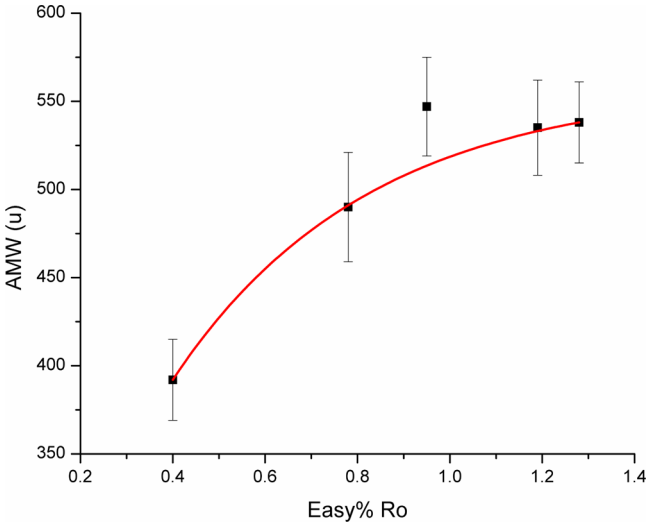

Figure 6. Average molecular weight (AMW) of the asphaltene samples as measured by L^2MS increases with maturity and then plateaus. The red trend line is a guide to the eye.

before hitting a plateau of approximately 540 g/mol for maturities above 0.95% EASY%Ro. Thus, asphaltene molecular weight appears to increase with maturity in the early stages of pyrolysis when bitumen is predominantly being created, and then the asphaltene molecular weight stays approximately constant with maturity in the later stages of pyrolysis when bitumen is predominantly being consumed. The molecular weight of even the mature asphaltene samples is slightly lower than that measured for petroleum asphaltenes from conventional reservoir rocks.[28,29]

Surface Assisted Laser Desorption Ionization (SALDI) Mass Spectrometry. SALDI mass spectra of the asphaltene samples are presented in Figure 7. The mass of the main peak

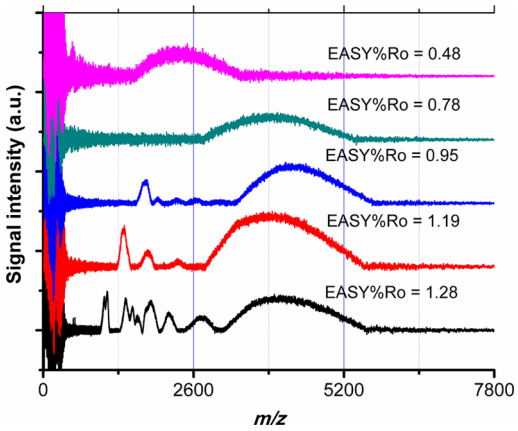

Figure 7. SALDI mass spectra of the asphaltene samples.

increases from near m/z = 2500 at low maturities to near m/z = 4000 at high maturities. This signal is assigned as asphaltene nanoaggregates in the Yen-Mullins model.[49] Nanoaggregates typically contain 6−8 molecules,[14,15] and the nanoaggregates in this study lie in that range (Table 1). The increase in asphaltene

Table 1. Average Molecular Mass (from L^2MS), Average Nanoaggregate Mass (from SALDI), and Average Nanoaggregate Number (Number of Molecules Per Nanoaggregate)

EASY%Ro (%)	molecular mass (Da)	nanoaggregate mass (Da)	nanoaggregate number
0.48	392	2403	6.1
0.78	490	3974	8.1
0.95	547	4548	8.3
1.19	535	4019	7.5
1.28	538	4525	8.4

nanoaggregate mass with maturity results mainly from an increase in the mass of individual molecules with maturity. The number of molecules contained in the nanoaggregate does not appear to increase significantly with maturity.

Sulfur K-Edge X-ray Absorption Near Edge Structure (XANES) Spectroscopy. Figure 8 presents the XANES spectra of the asphaltene samples, and Figure 9 presents the resulting sulfur speciations. Similar sulfur species, which are difficult to distinguish by XANES, are grouped to determine the sulfur speciation. In particular, the sulfide group comprises dibenzyl sulfide and diphenyl disulfide; the sulfoxide group comprises dibenzyl sulfoxide, dimethyl sulfoxide, and diphenyl sulfoxide; and the sulfonic group comprises isethionic acid and

DOI: 10.1021/acs.energyfuels.6b01238
Energy Fuels 2016, 30, 7025−7036

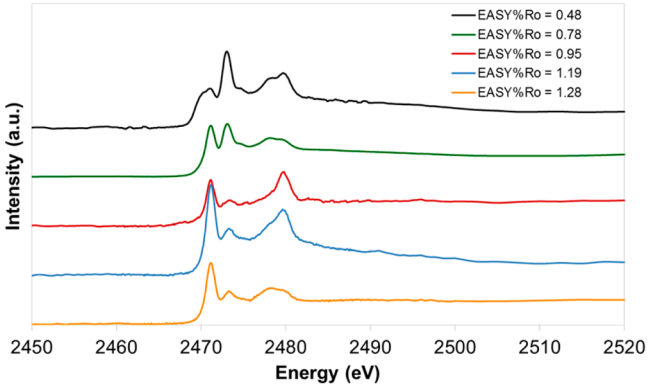

Figure 8. XANES spectra of the asphaltene samples. The intense peak at 2473 eV present in the immature samples but nearly absent in the high maturity samples corresponds to sulfoxide. Spectra are offset for clarity.

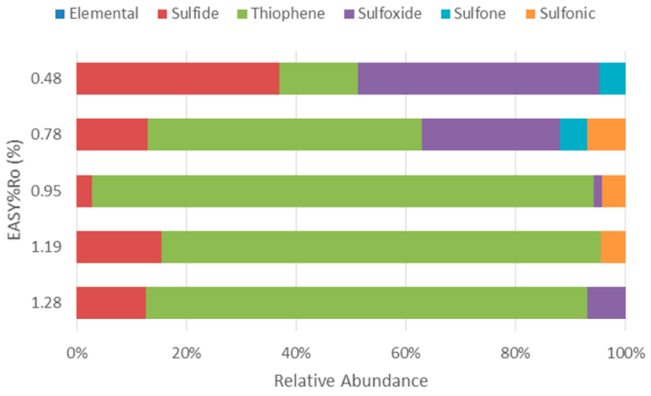

Figure 9. Sulfur speciation in the asphaltene samples as measured by XANES.

sulfonic acid. The sulfate signal was assumed to result from trace inorganic impurities and was removed from the speciation, as is often performed in XANES analysis of samples from unconventional resources.[8]

Sulfur speciation evolves systematically with maturity. The immature asphaltenes contain abundant sulfoxide, which decreases quickly during the early phase of maturation. Relatively abundant sulfide is also observed in the immature bitumen, which again decreases quickly during the early phase of maturation. As the sulfide and sulfoxide forms decrease in abundance, thiophenic sulfur increases with maturity, and at relatively high maturities there is more sulfur in the thiophene form than in all other forms combined. The trends in sulfur speciation observed here in the asphaltenes mirror those observed in the bitumens.[3] Similar to what was observed by L^2MS, most of the evolution in the composition of bitumen observable by XANES occurs at low maturity when bitumen is predominantly being produced. At relatively high maturities where bitumen is predominantly being consumed, the sulfur speciation of the asphaltenes is relatively constant.

Infrared (IR) Spectroscopy. IR spectra of the asphaltene samples are presented in Figure 10. Clear trends can be observed in the raw data, including an increase in the aromatic C═C and C−H bands and a decrease in the aliphatic C−H_x bands with maturity. The trends are expressed quantitatively in Figure 11 using several IR ratios as defined in Table 2. The definitions of the IR ratios used here are similar, but not identical, to those used by previous investigators.[7,93−95] The

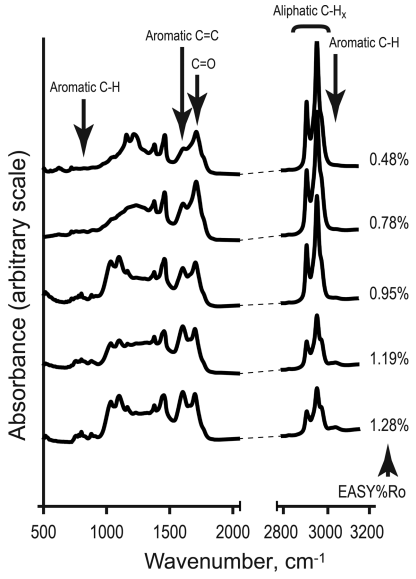

Figure 10. IR spectra of the asphaltene samples.

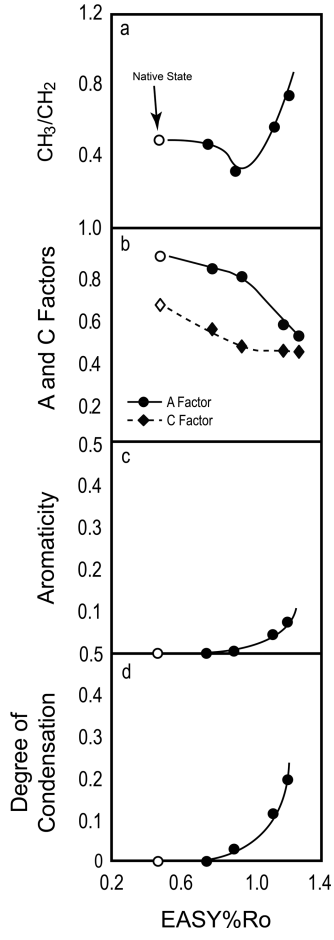

Figure 11. Asphaltene structural parameters determined by IR spectroscopy. Aromaticity refers to aromatic C−H groups, not all aromatic carbon (see Table 2 for details).

CH_3/CH_2 ratio is inversely proportional to the aliphatic chain length and is also impacted by the degree of branching. Aliphatic chains in asphaltenes appear to lengthen slightly with maturity at low maturities and then shorten more dramatically with maturity at higher maturities. The trend reverses at 0.95%

DOI: 10.1021/acs.energyfuels.6b01238
Energy Fuels 2016, 30, 7025−7036

Table 2. Definitions of the Structural Parameters Extracted from the IR Spectra[a]

metric name	description	formula
CH_3/CH_2 ratio	CH_3/CH_2	I_{2962}/I_{2925}
A-factor[b]	aliphatic C−H_2/[aliphatic C−H_2 + aromatic C=C]	$[I_{2857} + I_{2925}]/[I_{2857} + I_{2925} + I_{1600-1630}]$
C-factor[c]	C=O/[C=O + aromatic C=C]	$I_{1650-1770}/[I_{1650-1770} + I_{1600-1630}]$
aromaticity[d]	aromatic C−H/[aliphatic C−H_x + aromatic C−H]	$I_{3000-3100}/[I_{2800-3000} + I_{3000-3100}]$
degree of condensation	aromatic C−H/aromatic C=C	$I_{3000-3100}/I_{1600-1630}$

[a]In the formulas, I_x represents the area under the peak centered at wavenumber x, and I_{x-y} represents the sum of the areas under the peaks centered in the wavenumber range $x-y$. [b]Aromatic C=C represents the sum intensity of overlapping absorption bands centered between 1600 and 1630 cm^{-1} that are assigned to aromatic C=C stretches.[93] [c]C=O represents the sum intensities of three carbon−oxygen bands at 1650 cm^{-1} (quinone), 1710 cm^{-1} (ketone), and 1770 cm^{-1} (ester).[76,93] [d]Aliphatic C−H_x represents the sum intensities of five aliphatic C−H stretching bands at 2857, 2872, 2897, 2925, and 2956 cm^{-1} (symmetric CH_2, symmetric CH_3, CH, antisymmetric CH_2, and antisymmetric CH_3, respectively).[93]

EASY%Ro, where the dominant reaction switches from bitumen production to bitumen consumption.[3] This trend is not observed in analysis of the whole bitumen, as aliphatic chains in bitumen lengthen with maturity across the entire range of maturities studied here; however, the same trend was observed in the kerogen phase.[7]

Other trends in the composition of asphaltenes with maturity closely match those observed in bitumen.[7] The *A*-factor and the aromaticity both reflect the relative abundance of aromatic versus aliphatic carbon (aromaticity increases while the *A*-factor decreases with increasing abundance of aromatic carbon). Note that aromaticity as measured by IR includes only aromatic carbon bonded to hydrogen, different from other definitions of aromaticity such as that commonly used to interpret ^{13}C NMR spectra. Both metrics indicate that the asphaltenes become more aromatic with increasing maturity. This result is consistent with the decrease in H/C ratio with maturity as noted above, because H/C ratio has a strong and negative correlation with fraction of aromatic carbon in similar materials.[6,96] The *C*-factor reflects the oxygenated character of the asphaltenes and is found to decrease with maturity. A similar evolution of the *C*-factor with maturity was observed previously in asphaltenes from hydrous pyrolysis experiments,[80,84] and the decrease in oxygenated carbon observed here is consistent with the decrease in oxygenated sulfur (sulfoxide) observed in the XANES measurements (Figure 9). The degree of condensation (DOC) is proportional to the ratio of aromatic C−H to aromatic C=C. Aromatic C−H vibrations are barely detectable at low maturities even though aromatic C=C vibrations are clearly identified, indicating that most peripheral aromatic carbons are bonded to alkyl groups rather than terminated by hydrogens.[7] During early maturation, weak bonds beta to aromatic rings are broken, replacing long alkyl groups with methyl groups but still not creating a large fraction of aromatic C−H groups.[93] At high maturities those methyl groups are cleaved, creating a relatively large increase in the abundance of aromatic C−H groups, as shown by an increase in the DOC.

Figure 12 uses the same metrics as Figure 11 but formatted to be analogous to the van Krevelen diagram. The conventional H/C ratio (*y*-axis) is replaced by the *A*-factor, because both the H/C ratio and the *A*-factor increase with increasing fraction of aliphatic carbon; and the conventional O/C ratio (*x*-axis) is replaced by the *C*-factor, because both the O/C ratio and the *C*-factor increase with increasing fraction of oxygenated carbon. This representation illustrates how at low maturities the *C*-factor decreases rapidly with maturity while the *A*-factor decreases slowly, while at high maturities the *A*-factor decreases rapidly with maturity while the *C*-factor decreases slowly. This

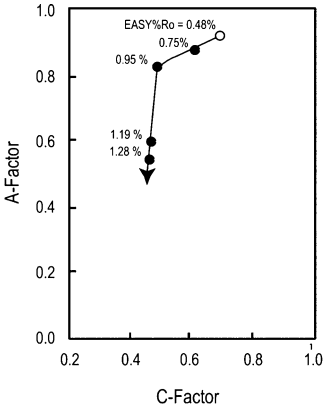

Figure 12. Pseudo van Krevelen diagram illustrating the evolution of the asphaltene composition as measured by IR spectroscopy.

same behavior was observed in the bitumen, although a subtle increase in the *C*-factor at low maturities was observed in the bitumen that is not observed here in the asphaltenes.

The broad carbonyl peak centered near 1700 cm^{-1} comprises several small peaks representing different bonding environments of the carbonyl. These small peaks can tentatively be assigned as quinone (centered at 1650 cm^{-1}), ketone (centered at 1710 cm^{-1}), and ester (centered at 1770 cm^{-1}).[7,76] The oxygen speciation of these asphaltenes can be estimated by deconvolving these peaks. As shown in Figure 13, the oxygen speciation appears to be relatively constant with maturity. This result is perhaps unexpected, as the shift toward more aromatic carbon observed in the aromaticity and in the *A*-factor, as well as in the sulfur speciation and the H/C ratio, is not observed in

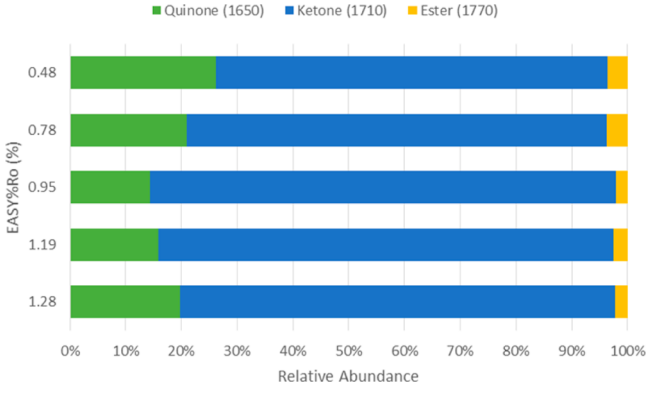

Figure 13. Oxygen speciation of the asphaltene samples as determined by IR spectroscopy. The approximate centers (cm^{-1}) of the assigned bands are listed.

DOI: 10.1021/acs.energyfuels.6b01238
Energy Fuels 2016, 30, 7025−7036

the quinone/ketone ratio. Nevertheless, the results indicate that the carbon−oxygen speciation of these asphaltenes holds relatively constant over the entire maturity range studied here.

DISCUSSION

The results indicate a systematic evolution in the composition of these asphaltenes with maturity. The evolution of asphaltene composition occurs in two phases: one phase at relatively low maturities (below 0.95% EASY%Ro) where the primary reaction involves bitumen formation and another phase at relatively high maturities (above 0.95% EASY%Ro) where the primary reaction involves bitumen consumption.

In the low maturity region, maturation primarily impacts the heteroatoms. The sulfur content of the asphaltenes decreases with maturity in this region. The speciation of sulfur also evolves, oxygenated sulfur (sulfoxide) decreases quickly as does sulfur bonded to aliphatic carbon (sulfide). The decreases in relative concentration of sulfoxide and sulfide are associated with an increase in the relative concentration of sulfur bonded to aromatic carbon (thiophene). The abundance of oxygenated carbon species (e.g., quinone, ketone, ester) also decreases during maturation, although the relative distribution among these functional groups appears to remain nearly the same. The molecular weight also evolves, increasing with maturity. On the other hand, changes in the carbon backbone are subtle. The abundance of aromatic C═C, the abundance of aromatic C−H, and the length of the aliphatic chains all stay relatively constant in this maturity region.

In the high maturity range, changes are more pronounced in the carbon backbone and less pronounced in the heteroatoms. The sulfur content is relatively constant and sulfur speciation is dominated by thiophenic forms at all maturities in this range. The abundance of oxygenated functionalities detected by IR spectroscopy remains relatively stable. Similarly, the asphaltene molecular weight holds relatively constant in this range. However, the aliphatic chain length shortens, the fraction of aliphatic carbon decreases, and the fraction of aromatic carbon increases with maturity in this region. The abundance of aromatic C−H bonds rises more quickly than the abundance of aromatic C═C bonds, reflecting relatively more frequent cleavage of aliphatic substitutions off aromatic rings than formation of aromatic C═C bonds at the highest maturities.

Two quantities appear to hold relatively constant over the entire maturity range studied here: (1) oxygen speciation (relative abundance of different carbon−oxygen functional groups) as determined by IR spectroscopy and (2) the number of asphaltene molecules that comprise an asphaltene nanoaggregate. While the nanoaggregate mass increases with maturity, the trend mirrors the increase in asphaltene molecular mass with maturity, and no change in the number of molecules per nanoaggregate is observed.

While many changes in the composition of asphaltenes are observed, these changes are not all independent. Asphaltenes are defined by their solubility (soluble in aromatic solvents but insoluble in aliphatic solvents). This definition mandates a balance in the intermolecular forces between asphaltenes: if intermolecular attraction is too strong, asphaltenes will not be soluble in aromatic solvent; if intermolecular attraction is too weak, asphaltenes will not be insoluble in aliphatic solvent.[97] The strength of intermolecular attractions is controlled by composition. Intermolecular attractive forces are generally stronger in organic molecules with greater molecular weight, higher fraction of aromatic carbon (which increases π-stacking attractions), and higher fraction of polar functional groups such as sulfoxide (which has a dipole moment near 4 D, double that of water).[8] If one of those factors increases, another will have to decrease in order to maintain the force balance. Here, the balance appears to be achieved by increasing molecular weight while decreasing sulfoxide content, both of which evolve most quickly at low maturities. This result suggests that dipole interactions contribute significantly to intermolecular interactions for immature asphaltenes. That result may be expected owing to unusually abundant sulfoxide in these asphaltenes and has been seen previously in other asphaltene samples with high sulfoxide.[27] At higher maturities, the sulfoxide has mostly disappeared and the dominant intermolecular attraction appears to be π-stacking, as is typically observed in petroleum asphaltenes from conventional reservoir rocks.[97]

CONCLUSIONS

The composition of asphaltenes derived from pyrolysis of Green River shale evolves systematically with maturity. At low maturities, where pyrolysis leads mainly to bitumen formation, the evolution of asphaltene composition is dominated by changes in the heteroatoms: carbon−oxygen, sulfur−oxygen (sulfoxide), and aliphatic carbon−sulfur (sulfide) bonds are lost, while the molecular weight increases. At high maturities, where pyrolysis leads mainly to bitumen consumption, the sulfur content, sulfur speciation, and molecular weight are relatively constant while the evolution in composition is dominated by changes in the carbon backbone: the abundance of aromatic relative to aliphatic carbon increases, the length of aliphatic chains shortens, and the relative abundance of aromatic C−H bonds increases greatly. The distribution of different carbon−oxygen functional groups appears relatively unchanged over the entire maturity range.

The compositional evolution of the asphaltenes can be compared to the compositional evolution of the bitumen.[3,6,7] Many of the maturity trends observed in asphaltenes mirror those observed in the bitumen; for example, aromaticity increases and sulfoxide content decreases with maturity in both asphaltenes and bitumen. However, some trends observed in asphaltenes are not observed in bitumen; for example, aliphatic chains in bitumen lengthen with maturity over the full range investigated here,[7] while aliphatic chains in asphaltenes lengthen subtly at low maturities before shortening significantly at higher maturities. These results demonstrate how the evolution of the asphaltene fraction of bitumen can differ from that of the maltene fraction.

The trends observed here in the composition of asphaltenes from pyrolysis are not necessarily expected in the composition of petroleum asphaltenes from naturally occurring reservoir rocks that are not also source rocks. Asphaltenes formed in natural source rock are expelled in a liquid phase (primary migration) and migrate (secondary migration) into conventional reservoir rocks. The reservoir rocks are typically shallower and colder than the source rocks, so the pyrolysis of asphaltenes slows at the moment of expulsion.[98] While the source rock continues to mature, filling the reservoir with higher-maturity oil (which contains relatively low concentration of high-maturity asphaltenes), the composition of the asphaltenes in the reservoir rock changes slowly. In contrast, in the pyrolysis experiments employed here, oil is expelled as a vapor so the asphaltenes remain primarily in the high-temperature reactor until the end of the pyrolysis. As a result, the asphaltenes studied here effectively have been exposed to a

DOI: 10.1021/acs.energyfuels.6b01238
Energy Fuels 2016, 30, 7025−7036

larger range of thermal histories than asphaltenes residing in conventional reservoir rock. The asphaltenes studied here are thus expected to be more representative of those occurring in unconventional resources such as some tight-oil formations where the asphaltenes have not undergone primary migration but instead remain in the source rock throughout the maturation process. These results suggest that compositional analysis of asphaltenes could be used to estimate the maturity of the asphaltene fraction, particularly for source rocks.

Compositional evolution during pyrolysis is normally described by a network of chemical reactions, dictated by activation energies and frequency factors. Changes in pyrolysis kinetics of natural asphaltenes of varying maturities have been observed previously,[99] consistent with the changes in asphaltene composition as described here. While the concept of a reaction network is a powerful way to understand the asphaltene evolution studied here, asphaltene composition is also impacted by intermolecular interactions. By limiting the study to the fraction of material that dissolves in aromatic solvent but not in aliphatic solvent (the definition of asphaltenes), additional constraints are imposed. If the composition prescribes too strong intermolecular interactions, the material will be not soluble in aromatic solvent; while if the composition prescribes too weak intermolecular interactions, the material will be not insoluble in aliphatic solvent. As a result, changes in the composition of asphaltenes cannot be independent of one another. Here, the constraint is manifest as a decrease in sulfoxide content (weakening intermolecular forces by reducing dipole interactions) concurrent with an increase in molecular weight (strengthening intermolecular forces) at low maturities. The strength of intermolecular interactions also controls the size of noncovalently bonded asphaltene nanoaggregates, which are held together by these intermolecular interactions. As a result of the balanced intermolecular interactions achieved by these simultaneous changes in composition, the nanoaggregate number (number of asphaltene molecules in a nanoaggregate) holds nearly constant over the range of maturities, even while the nanoaggregate mass varies.

AUTHOR INFORMATION

Corresponding Author

*E-mail: apomerantz@slb.com.

Present Address

#T.B.B.: Colorado State University, Fort Collins, CO 80521.

Notes

The authors declare no competing financial interest.

ACKNOWLEDGMENTS

The authors would like to thank Total S. A. and Schlumberger for their support of this work and Pierre Allix of Total in particular. The Total support came both by providing AMSO oil shale samples and through the Stanford-Total Enhanced Modeling of Source Rocks (STEMS) project. Use of the Advanced Photon Source, an Office of Science User Facility operated for the U.S. Department of Energy Office of Science by Argonne National Laboratory, was supported by DOE under Contract No. DE-AC02-06CH11357. We thank Andrew Judd of Schlumberger for assistance in preparing Figure 3.

REFERENCES

(1) Durand, B. Sedimentary organic matter and kerogen. Definition and quantitative importance of kerogen. In *Kerogen: Insoluble Organic Matter from Sedimentary Rocks*, Durand, B., Ed. Editions Technip: Paris, France, 1980.

(2) Burnham, A. K.; Braun, R. L. Development of a detailed model of petroleum formation, destruction, and expulsion from lacustrine and marine source rocks. *Org. Geochem.* **1990**, *16*, 27−39.

(3) Le Doan, T. V.; Bostrom, N. W.; Burnham, A. K.; Kleinberg, R. L.; Pomerantz, A. E.; Allix, P. Green River Oil Shale Pyrolysis: Semi-Open Conditions. *Energy Fuels* **2013**, *27*, 6447−6459.

(4) Kelemen, S. R.; Afeworki, M.; Gorbaty, M. L.; Sansone, M.; Kwiatek, P. J.; Walters, C. C.; Freund, H.; Siskin, M.; Bence, A. E.; Curry, D. J.; Solum, M. S.; Pugmire, R. J.; Vandenbroucke, M.; Leblond, M.; Behar, F. Direct Characterization of Kerogen by X-ray and Solid-State ^{13}C Nuclear Magnetic Resonance Methods. *Energy Fuels* **2007**, *21*, 1548−1561.

(5) van Krevelen, D. W. *Coal: Typology, Chemistry, Physics - Constitution*; Elsevier Science: Amsterdam, The Netherlands, 1961.

(6) Feng, Y.; Le Doan, T. V.; Pomerantz, A. E. The Chemical Composition of Bitumen in Pyrolyzed Green River Oil Shale: Characterization by ^{13}C NMR Spectroscopy. *Energy Fuels* **2013**, *27*, 7314−7323.

(7) Craddock, P. R.; Le Doan, T. V.; Bake, K. D.; Polyakov, M.; Charsky, A.; Pomerantz, A. E. Evolution of Kerogen and Bitumen during Thermal Maturation via Semi-Open Pyrolysis Investigated by Infrared Spectroscopy. *Energy Fuels* **2015**, *29*, 2197−2210.

(8) Pomerantz, A. E.; Bake, K. D.; Craddock, P. R.; Kurzenhauser, K. W.; Kodalen, B. G.; Mitra-Kirtley, S.; Bolin, T. Sulfur Speciation in Kerogen and Bitumen from Gas and Oil Shales. *Org. Geochem.* **2014**, *68*, 5−12.

(9) Tissot, B.; Welte, D. *Petroleum Formation and Occurrence*, 2nd ed.; Springer: Berlin, Germany, 1984; p 702.

(10) Peters, K. E.; Walters, C. C.; Moldowan, J. M. *The Biomarker Guide*, 2nd ed.; Cambridge University Press: Cambridge, U.K., 2005; Vol. *1*.

(11) Herod, A. A.; Bartle, K. D.; Kandiyoti, R. Characterization of Heavy Hydrocarbons by Chromatographic and Mass Spectrometric Methods: An Overview. *Energy Fuels* **2007**, *21*, 2176−2203.

(12) Mullins, O. C.; Martínez-Haya, B.; Marshall, A. G. Contrasting Perspective on Asphaltene Molecular Weight. This Comment vs the Overview of A. A. Herod, K. D. Bartle, and R. Kandiyoti. *Energy Fuels* **2008**, *22*, 1765−1773.

(13) Pomerantz, A. E. Toward Molecule-Specific Geochemistry of Heavy Ends: Application to the Upstream Oil Industry. *Ind. Eng. Chem. Res.* **2016**, *55*, 4403−4414.

(14) Mullins, O. C. The Modified Yen Model. *Energy Fuels* **2010**, *24*, 2179−2207.

(15) Mullins, O. C.; Sabbah, H.; Eyssautier, J.; Pomerantz, A. E.; Barré, L.; Andrews, A. B.; Ruiz-Morales, Y.; Mostowfi, F.; McFarlane, R.; Goual, L.; Lepkowicz, R.; Cooper, T.; Orbulescu, J.; Leblanc, R. M.; Edwards, J.; Zare, R. N. Advances in Asphaltene Science and the Yen−Mullins Model. *Energy Fuels* **2012**, *26*, 3986−4003.

(16) Freed, D. E.; Mullins, O. C.; Zuo, J. Y. Theoretical Treatment of Asphaltene Gradients in the Presence of GOR Gradients. *Energy Fuels* **2010**, *24*, 3942−3949.

(17) Zuo, J. Y.; Mullins, O. C.; Mishra, V.; Garcia, G.; Dong, C.; Zhang, D. Asphaltene Grading and Tar Mats in Oil Reservoirs. *Energy Fuels* **2012**, *26*, 1670−1680.

(18) Mullins, O. C.; Seifert, D. J.; Zuo, J. Y.; Zeybek, M. Clusters of Asphaltene Nanoaggregates Observed in Oilfield Reservoirs. *Energy Fuels* **2013**, *27*, 1752−1761.

(19) Zuo, J. Y.; Mullins, O. C.; Freed, D.; Elshahawi, H.; Dong, C.; Seifert, D. J. Advances in the Flory−Huggins−Zuo Equation of State for Asphaltene Gradients and Formation Evaluation. *Energy Fuels* **2013**, *27*, 1722−1735.

(20) Dong, C.; Petro, D.; Pomerantz, A. E.; Nelson, R. K.; Latifzai, A. S.; Nouvelle, X.; Zuo, J. Y.; Reddy, C. M.; Mullins, O. C. New

DOI: 10.1021/acs.energyfuels.6b01238
Energy Fuels 2016, 30, 7025−7036

thermodynamic modeling of reservoir crude oil. *Fuel* **2014**, *117*, 839−850.
(21) Freed, D. E.; Mullins, O. C.; Zuo, J. Y. Heuristics for Equilibrium Distributions of Asphaltenes in the Presence of GOR Gradients. *Energy Fuels* **2014**, *28*, 4859−4869.
(22) Mullins, O. C.; Pomerantz, A. E.; Zuo, J. Y.; Dong, C. Downhole fluid analysis and asphaltene science for petroleum reservoir evaluation. *Annu. Rev. Chem. Biomol. Eng.* **2014**, *5*, 325−45.
(23) Zuo, J. Y.; Jackson, R.; Agarwal, A.; Herold, B.; Kumar, S.; Santo, I. D.; Dumont, H.; Ayan, C.; Beardsell, M.; Mullins, O. C. Diffusion Model Coupled with the Flory−Huggins−Zuo Equation of State and Yen−Mullins Model Accounts for Large Viscosity and Asphaltene Variations in a Reservoir Undergoing Active Biodegradation. *Energy Fuels* **2015**, *29*, 1447−1460.
(24) Wang, K.; Zuo, J. Y.; Chen, Y.; Mullins, O. C. The dynamic Flory-Huggins-Zuo equation of state. *Energy* **2015**, *91*, 430−440.
(25) Rane, J. P.; Zarkar, S.; Pauchard, V.; Mullins, O. C.; Christie, D.; Andrews, A. B.; Pomerantz, A. E.; Banerjee, S. Applicability of the Langmuir Equation of State for Asphaltene Adsorption at the Oil−Water Interface: Coal-Derived, Petroleum, and Synthetic Asphaltenes. *Energy Fuels* **2015**, *29*, 3584−3590.
(26) Groenzin, H.; Mullins, O. C. Asphaltene Molecular Size and Structure. *J. Phys. Chem. A* **1999**, *103*, 11237−11245.
(27) Groenzin, H.; Mullins, O. C. Molecular Size and Structure of Asphaltenes from Various Sources. *Energy Fuels* **2000**, *14*, 677−684.
(28) Pomerantz, A. E.; Hammond, M. R.; Morrow, A. L.; Mullins, O. C.; Zare, R. N. Two-Step Laser Mass Spectrometry of Asphaltenes. *J. Am. Chem. Soc.* **2008**, *130*, 7216−7217.
(29) Pomerantz, A. E.; Hammond, M. R.; Morrow, A. L.; Mullins, O. C.; Zare, R. N. Asphaltene Molecular-Mass Distribution Determined by Two-Step Laser Mass Spectrometry. *Energy Fuels* **2009**, *23*, 1162−1168.
(30) Sabbah, H.; Morrow, A. L.; Pomerantz, A. E.; Zare, R. N. Evidence for Island Structures as the Dominant Architecture of Asphaltenes. *Energy Fuels* **2011**, *25*, 1597−1604.
(31) Sabbah, H.; Pomerantz, A. E.; Wagner, M.; Müllen, K.; Zare, R. N. Laser Desorption Single-Photon Ionization of Asphaltenes: Mass Range, Compound Sensitivity, and Matrix Effects. *Energy Fuels* **2012**, *26*, 3521−3526.
(32) Sabbah, H.; Morrow, A. L.; Pomerantz, A. E.; Mullins, O. C.; Tan, X.; Gray, M. R.; Azyat, K.; Tykwinski, R. R.; Zare, R. N. Comparing Laser Desorption/Laser Ionization Mass Spectra of Asphaltenes and Model Compounds. *Energy Fuels* **2010**, *24*, 3589−3594.
(33) Pomerantz, A. E.; Wu, Q.; Mullins, O. C.; Zare, R. N. Laser-Based Mass Spectrometric Assessment of Asphaltene Molecular Weight, Molecular Architecture, and Nanoaggregate Number. *Energy Fuels* **2015**, *29*, 2833−2842.
(34) Hortal, A. R.; Martínez-Haya, B.; Lobato, M. D.; Pedrosa, J. M.; Lago, S. On the determination of molecular weight distributions of asphaltenes and the aggregates in laser desorption ionization experiments. *J. Mass Spectrom.* **2006**, *41*, 960−968.
(35) Hortal, A. R.; Hurtado, P.; Martínez-Haya, B.; Mullins, O. C. Molecular Weight Distributions of Coal and Petroleum Asphaltenes from Laser Desorption/Ionization Experiments. *Energy Fuels* **2007**, *21*, 2863−2868.
(36) Martínez-Haya, B.; Hortal, A. R.; Hurtado, P.; Lobato, M. D.; Pedrosa, J. M. Laser desorption/ionization determination of molecular weight distributions of polyaromatic carbonaceous compounds and their aggregates. *J. Mass Spectrom.* **2007**, *42*, 701−713.
(37) Tang, W.; Hurt, M. R.; Sheng, H.; Riedeman, J. S.; Borton, D. J.; Slater, P.; Kenttämaa, H. I. Structural Comparison of Asphaltenes of Different Origins Using Multi-stage Tandem Mass Spectrometry. *Energy Fuels* **2015**, *29*, 1309−1314.
(38) Ruiz-Morales, Y.; Wu, X.; Mullins, O. C. Electronic Absorption Edge of Crude Oils and Asphaltenes Analyzed by Molecular Orbital Calculations with Optical Spectroscopy. *Energy Fuels* **2007**, *21*, 944−952.
(39) Ruiz-Morales, Y.; Mullins, O. C. Polycyclic Aromatic Hydrocarbons of Asphaltenes Analyzed by Molecular Orbital Calculations with Optical Spectroscopy. *Energy Fuels* **2007**, *21*, 256−265.
(40) Andrews, A. B.; Edwards, J. C.; Pomerantz, A. E.; Mullins, O. C.; Nordlund, D.; Norinaga, K. Comparison of Coal-Derived and Petroleum Asphaltenes by ^{13}C Nuclear Magnetic Resonance, DEPT, and XRS. *Energy Fuels* **2011**, *25*, 3068−3076.
(41) Dutta Majumdar, R.; Gerken, M.; Mikula, R.; Hazendonk, P. Validation of the Yen−Mullins Model of Athabasca Oil-Sands Asphaltenes using Solution-State1H NMR Relaxation and 2D HSQC Spectroscopy. *Energy Fuels* **2013**, *27*, 6528−6537.
(42) Alemany, L. B.; Verma, M.; Billups, W. E.; Wellington, S. L.; Shammai, M. Solid- and Solution-State Nuclear Magnetic Resonance Analyses of Ecuadorian Asphaltenes: Quantitative Solid-State Aromaticity Determination Supporting the "Island" Structural Model. Aliphatic Structural Information from Solution-State1H−13C Heteronuclear Single-Quantum Coherence Experiments. *Energy Fuels* **2015**, *29*, 6317−6329.
(43) Schuler, B.; Meyer, G.; Pena, D.; Mullins, O. C.; Gross, L. Unraveling the Molecular Structures of Asphaltenes by Atomic Force Microscopy. *J. Am. Chem. Soc.* **2015**, *137*, 9870−6.
(44) Speight, J. G. Chemical and Physical Studies of Petroleum Asphaltenes. In *Developments in Petroleum Science*; Elsevier Science B.V.: Amsterdam, The Netherlands, 1994, Vol. *40*, Part A; pp 7−65.
(45) Burnham, A. K.; McConaghy, J. R. Semi-Open Pyrolysis of Oil Shale from the Garden Gulch Member of the Green River Formation. *Energy Fuels* **2014**, *28*, 7426−7439.
(46) Sweeney, J. J.; Burnham, A. K. Evaluation of a Simple Model of Vitrinite Reflectance Based on Chemical Kinetics. *AAPG Bull.* **1990**, *74*, 1559−1570.
(47) Hurtado, P.; Gámez, F.; Martínez-Haya, B. One- and Two-Step Ultraviolet and Infrared Laser Desorption Ionization Mass Spectrometry of Asphaltenes. *Energy Fuels* **2010**, *24*, 6067−6073.
(48) Wu, Q.; Pomerantz, A. E.; Mullins, O. C.; Zare, R. N. Minimization of Fragmentation and Aggregation by Laser Desorption Laser Ionization Mass Spectrometry. *J. Am. Soc. Mass Spectrom.* **2013**, *24*, 1116−1122.
(49) Wu, Q.; Pomerantz, A. E.; Mullins, O. C.; Zare, R. N. Laser-Based Mass Spectrometric Determination of Aggregation Numbers for Petroleum- and Coal-Derived Asphaltenes. *Energy Fuels* **2014**, *28*, 475−482.
(50) Wu, Q.; Seifert, D. J.; Pomerantz, A. E.; Mullins, O. C.; Zare, R. N. Constant Asphaltene Molecular and Nanoaggregate Mass in a Gravitationally Segregated Reservoir. *Energy Fuels* **2014**, *28*, 3010−3015.
(51) Maechling, C. R.; Clemett, S. J.; Engelke, F.; Zare, R. N. Evidence for thermalization of surface-desorbed molecules at heating rates of 10^8 K/s. *J. Chem. Phys.* **1996**, *104*, 8768−8776.
(52) Hanley, L.; Zimmermann, R. Light and molecular ions: the emergence of vacuum UV single-photon ionization in MS. *Anal. Chem.* **2009**, *81*, 4174−82.
(53) Hammond, M. R.; Zare, R. N. Identifying the source of a strong fullerene envelope arising from laser desorption mass spectrometric analysis of meteoritic insoluble organic matter. *Geochim. Cosmochim. Acta* **2008**, *72*, 5521−5529.
(54) de Hoffmann, E.; Stroobant, V. *Mass Spectrometry: Principles and Applications*, 3rd ed.; John Wiley & Sons, Ltd.: Chichester, U.K., 2007; p 489.
(55) Spiro, C. L.; Wong, J.; Lytle, F. W.; Greegor, R. B.; Maylotte, D. H.; Lamson, S. H. X-ray Absorption Spectroscopic Investigation of Sulfur Sites in Coal: Organic Sulfur Indentification. *Science* **1984**, *226*, 48−50.
(56) Huffman, G. P.; Mitra-Kirtley, S.; Huggins, F. E.; Shah, N.; Vaidya, S.; Lu, F. Quantitative Analysis of All Major Forms of Sulfur in Coal by X-ray Absorption Fine Structure Spectroscopy. *Energy Fuels* **1991**, *5*, 574−581.
(57) Gorbaty, M. L.; Kelemen, S. R.; George, G. N.; Kwiatek, P. J. Characterization and thermal reactivity of oxidized organic sulfur forms in coals. *Fuel* **1992**, *71*, 1255−1264.

DOI: 10.1021/acs.energyfuels.6b01238
Energy Fuels 2016, 30, 7025−7036

(58) Wiltfong, R.; Mitra-Kirtley, S.; Mullins, O. C.; Andrews, A. B.; Fujisawa, G.; Larsen, J. W. Sulfur Speciation in Different Kerogen by XANES Spectroscopy. *Energy Fuels* **2005**, *19*, 1971−1976.
(59) Kelemen, S. R.; Sansone, M.; Walters, C. C.; Kwiatek, P. J.; Bolin, T. Thermal transformations of organic and inorganic sulfur in Type II kerogen quantified by S-XANES. *Geochim. Cosmochim. Acta* **2012**, *83*, 61−78.
(60) Kelemen, S. R.; Walters, C. C.; Kwiatek, P. J.; Freund, H.; Afeworki, M.; Sansone, M.; Lamberti, W. A.; Pottorf, R. J.; Machel, H. G.; Peters, K. E. Characterization of solid bitumens originating from thermal chemical alteration and thermochemical sulfate reduction. *Geochim. Cosmochim. Acta* **2010**, *74*, 5305−5332.
(61) Greenfield, M. L.; Byrne, M.; Mitra-Kirtley, S.; Kercher, E. M.; Bolin, T. B.; Wu, T.; Craddock, P. R.; Bake, K. D.; Pomerantz, A. E. XANES measurements of sulfur chemistry during asphalt oxidation. *Fuel* **2015**, *162*, 179−185.
(62) Mitra-Kirtley, S.; Mullins, O. C.; Ralston, C. Y.; Sellis, D.; Pareis, C. Determination of Sulfur Species in Asphaltene, Resin, and Oil Fractions of Crude Oils. *Appl. Spectrosc.* **1998**, *52*, 1522−1525.
(63) Pomerantz, A. E.; Seifert, D. J.; Bake, K. D.; Craddock, P. R.; Mullins, O. C.; Kodalen, B. G.; Mitra-Kirtley, S.; Bolin, T. B. Sulfur Chemistry of Asphaltenes from a Highly Compositionally Graded Oil Column. *Energy Fuels* **2013**, *27*, 4604−4608.
(64) George, G. N.; Gorbaty, M. L. Sulfur K-Edge X-ray Absorption Spectroscopy of Petroleum Asphaltenes and Model Compounds. *J. Am. Chem. Soc.* **1989**, *111*, 3182−3186.
(65) Waldo, G. S.; Mullins, O. C.; Penner-Hahn, J. E.; Cramer, S. P. Determination of the chemical environment of sulphur in petroleum asphaltenes by X-ray absorption spectroscopy. *Fuel* **1992**, *71*, 53−57.
(66) Waldo, G. S.; Carlson, R. M. K.; Moldowan, J. M.; Peters, K. E.; Penner-Hahn, J. E. Sulfur speciation in heavy petroleums: Information from X-ray absorption near-edge structure. *Geochim. Cosmochim. Acta* **1991**, *55*, 801−814.
(67) Pickering, I. J.; George, G. N.; Yu, E. Y.; Brune, D. C.; Tuschak, C.; Overmann, J.; Beatty, J. T.; Prince, R. C. Analysis of Sulfur Biochemistry of Sulfur Bacteria Using X-ray Absorption Spectroscopy. *Biochemistry* **2001**, *40*, 8138−8145.
(68) Behyan, S.; Hu, Y.; Urquhart, S. G. Sulfur 1s near-edge x-ray absorption fine structure (NEXAFS) of thiol and thioether compounds. *J. Chem. Phys.* **2011**, *134*, 244304.
(69) Frank, P.; Hedman, B.; Carlson, R. M. K.; Tyson, T. A.; Roe, A. L.; Hodgson, K. O. A Large Reservoir of Sulfate and Sulfonate Resides within Plasma Cells from *Ascidia ceratodes*, Revealed by X-ray Absorption Near-Edge Structure Spectroscopy. *Biochemistry* **1987**, *26*, 4975−4979.
(70) George, G. N.; Hackett, M. J.; Sansone, M.; Gorbaty, M. L.; Kelemen, S. R.; Prince, R. C.; Harris, H. H.; Pickering, I. J. Long-range chemical sensitivity in the sulfur K-edge X-ray absorption spectra of substituted thiophenes. *J. Phys. Chem. A* **2014**, *118*, 7796−802.
(71) Mijovilovich, A.; Pettersson, L. G.; Mangold, S.; Janousch, M.; Susini, J.; Salome, M.; de Groot, F. M. F.; Weckhuysen, B. M. The Interpretation of Sulfur K-Edge XANES Spectra: A Case Study on Thiophenic and Aliphatic Sulfur Compounds. *J. Phys. Chem. A* **2009**, *113*, 2750−2756.
(72) Lewan, M. D. Sulphur-radical control on petroleum formation rates. *Nature* **1998**, *391*, 164−166.
(73) Mitra-Kirtley, S.; Mullins, O. C.; Pomerantz, A. E., Sulfur and Nitrogen Chemical Speciation in Crude Oils and Related Carbonaceous Materials. In *Applying Nanotechnology to the Desulfurization Process in Petroleum Engineering*; Saleh, T. A., Ed. Engineering Science Reference: Hershey, PA, 2016; pp 53−83.
(74) Sekiyama, H.; Kosugi, N.; Kuroda, H.; Ohta, T. Sulfur K-Edge Absorption Spectra of Na_2SO_4, Na_2SO_3, $Na_2S_2O_3$, and $Na_2S_2O_x$ (x = 5−8). *Bull. Chem. Soc. Jpn.* **1986**, *59*, 575−579.
(75) Rosen, P.; Vogel, H.; Cunningham, L.; Hahn, A.; Hausmann, S.; Pienitz, R.; Zolitschka, B.; Wagner, B.; Persson, P. Universally applicable model for the quantitative determination of lake sediment composition using fourier transform infrared spectroscopy. *Environ. Sci. Technol.* **2011**, *45*, 8858−65.
(76) Painter, P. C.; Snyder, R. W.; Starsinic, M.; Coleman, M. M.; Kuehn, D. W.; Davis, A. Concerning the Application of FT-IR to the Study of Coal: A Critical Assessment of Band Assignments and the Application of Spectral Analysis Programs. *Appl. Spectrosc.* **1981**, *35*, 475−485.
(77) Ibarra, J. V.; Munoz, E.; Moliner, R. FTIR study of the evolution of coal structure during the coalification process. *Org. Geochem.* **1996**, *24*, 725−735.
(78) Michels, R.; Burkle, V.; Mansuy, L.; Langlois, E.; Ruau, O.; Landais, P. Role of Polar Compounds as Source of Hydrocarbons and Reactive Medium during the Artificial Maturation of Mahakam Coal. *Energy Fuels* **2000**, *14*, 1059−1071.
(79) Durand, B.; Espitalie, J. Geochemical studies on the organic matter from the Douala Basin (Cameroon)–II. Evolution of kerogen. *Geochim. Cosmochim. Acta* **1976**, *40*, 801−808.
(80) Christy, A. A.; Kvalheim, O. M.; Øygard, K.; Dahl, B.; Karstang, T. V. Maturity of kerogen and asphaltenes determined by partial-least-squares (PLS) calibration and target projection of diffuse reflectance Fourier transformed infrared spectra. *Org. Geochem.* **1991**, *17*, 63−74.
(81) Rouxhet, P. G.; Robin, P. L.; Nicaise, G., Characterization of kerogens and their evolution by infrared spectroscopy. In *Kerogen: Insoluble Organic Matter from Sedimentary Rocks*, Durand, B., Ed. Editions Technip: Paris, France, 1980.
(82) Lis, G. P.; Mastalerz, M.; Schimmelmann, A.; Lewan, M. D.; Stankiewicz, B. A. FTIR absorption indices for thermal maturity in comparison with vitrinite reflectance R0 in type-II kerogens from Devonian black shales. *Org. Geochem.* **2005**, *36*, 1533−1552.
(83) Jin, X.; Han, R.; Cui, Y.; Glover, C. J. Fast-Rate−Constant-Rate Oxidation Kinetics Model for Asphalt Binders. *Ind. Eng. Chem. Res.* **2011**, *50*, 13373−13379.
(84) Christy, A. A.; Hopland, A. L.; Barth, T.; Kvalheim, O. M. Quantitative determination of thermal maturity in sedimentary organic matter by diffuse reflectance infrared spectroscopy of asphaitenes. *Org. Geochem.* **1989**, *14*, 77−81.
(85) Barth, T.; Seim, M.; Christy, A. A.; Kvalheim, O. M. Maturity trends in asphaltenes from pyrolysed source rocks and natural coals–multivariate modelling of diffuse reflectance Fourier-transform infrared spectra. *Org. Geochem.* **1995**, *23*, 139−158.
(86) Michaelian, K. H.; Friesen, W. I. Photoacoustic FT-i.r. spectra of separated western Canadian coal macerals: Analysis of the CH stretching region by curve-fitting and deconvolution. *Fuel* **1990**, *69*, 1271−1275.
(87) Ferralis, N.; Liu, Y.; Bake, K. D.; Pomerantz, A. E.; Grossman, J. C. Direct correlation between aromatization of carbon-rich organic matter and its visible electronic absorption edge. *Carbon* **2015**, *88*, 139−147.
(88) Ruiz-Morales, Y. HOMO-LUMO Gap as an Index of Molecular Size and Structure for Polycyclic Aromatic Hydrocarbons (PAHs) and Asphaltenes: A Theoretical Study. I. *J. Phys. Chem. A* **2002**, *106*, 11283−11308.
(89) Keym, M.; Dieckmann, V. PREDICTING THE TIMING AND CHARACTERISTICS OF PETROLEUM FORMATION USING TAR MATS AND PETROLEUM ASPHALTENES: A CASE STUDY FROM THE NORTHERN NORTH SEA. *J. Pet. Geol.* **2006**, *29*, 273−296.
(90) Bunger, J. W.; Cogswell, D. E. Characteristics of Tar Sand Bitumen Asphaltenes as Studied by Conversion of Bitumen by Hydropyrolysis. In *Chemistry of Asphaltenes*; American Chemical Society: Washington, DC, 1982; Vol. *195*, pp 219−236.
(91) Li, K.; Vasiliu, M.; McAlpin, C. R.; Yang, Y.; Dixon, D. A.; Voorhees, K. J.; Batzle, M.; Liberatore, M. W.; Herring, A. M. Further insights into the structure and chemistry of the Gilsonite asphaltene from a combined theoretical and experimental approach. *Fuel* **2015**, *157*, 16−20.
(92) Behar, F.; Pelet, R.; Roucache, J. Geochemistry of asphaltenes. *Org. Geochem.* **1984**, *6*, 587−595.
(93) Lin, R.; Ritz, G. P. Studying individual macerals using i.r. microspectroscopy, and implications on oil versus gas/condensate

DOI: 10.1021/acs.energyfuels.6b01238
Energy Fuels 2016, 30, 7025−7036

proneness and "low-rank" generation. *Org. Geochem.* **1993**, *20*, 695−706.
(94) Ganz, H.; Kalkreuth, W. Application of infrared spectroscopy to the classification of kerogen types and the evaluation of source rock and oil shale potentials. *Fuel* **1987**, *66*, 708−711.
(95) Ganz, H. H.; Kalkreuth, W. IR classification of kerogen type, thermal maturation, hydrocarbon potential and lithological characteristics. *Journal of Southeast Asian Earth Science* **1991**, *5*, 19−28.
(96) Maciel, G. E.; Bartuska, V. J.; Miknis, F. P. Characterization of organic material in coal by proton-decoupled ^{13}C nuclear magnetic resonance with magic-angle spinning. *Fuel* **1979**, *58*, 391−394.
(97) Buenrostro-Gonzalez, E.; Groenzin, H.; Lira-Galeana, C.; Mullins, O. C. The Overriding Chemical Principles that Define Asphaltenes. *Energy Fuels* **2001**, *15*, 972−978.
(98) Curiale, J. A.; Curtis, J. B. Organic geochemical applications to the exploration for source-rock reservoirs − A review. *Journal of Unconventional Oil and Gas Resources* **2016**, *13*, 1−31.
(99) di Primio, R.; Horsfield, B.; Guzman-Vega, M. A. Determining the temperature of petroleum formation from the kinetic properties of petroleum asphaltenes. *Nature* **2000**, *406*, 173−176.

DOI: 10.1021/acs.energyfuels.6b01238
Energy Fuels 2016, 30, 7025−7036